



OPEN Numerical study on small hole leakage and diffusion of hydrogen in buried pipelines

Longfei Dong^{1,2}✉, Xin Pang¹ & Rui Zhang^{1,2}

In this paper, a numerical simulation method is systematically employed to study the diffusion behavior of pure hydrogen and hydrogen-blended natural gas during small-hole leakage from buried pipelines. The study focuses on the quantitative effects of operating parameters, leakage orifice characteristics, burial depth, and soil properties on leakage dynamics and surface hazard time. The results indicate that increasing soil porosity and particle size significantly accelerates the diffusion rate, reducing the time required for hydrogen to reach the Lower Explosive Limit (LEL, 4%) at the ground surface from 130 s (Porosity 0.43) to 75 s (Porosity 0.55). Upward-oriented leakage is confirmed to be the highest risk scenario, leading to the fastest concentration saturation due to buoyant forces. Furthermore, the diffusion performance of the leakage orifice is ranked as axial rectangular slit > radial rectangular slit > circular hole, demonstrating that shape and aspect ratio critically influence the diffusion range and surface ignition risk. This research provides a quantitative foundation and dimensionless correlations for hazard assessment and safety management of low-pressure hydrogen and hydrogen-blended natural gas distribution pipelines.

Keywords Pure hydrogen, Hydrogen blending, Buried pipeline, Leakage and diffusion, Monitoring

As global demand for clean energy continues to rise, the importance of natural gas within the energy structure has become increasingly prominent. Natural gas is widely regarded as a relatively clean fossil fuel, and its potential to reduce greenhouse gas emissions makes it a crucial transitional bridge toward renewable energy sources. According to Li¹, while the use of natural gas contributes to the optimization of the energy structure, it can also exacerbate the greenhouse effect during its utilization process. Therefore, the green development of natural gas is particularly important.

However, frequent pipeline leakage incidents during the transportation and utilization of natural gas pose serious risks and losses to the environment and society. Meng² pointed out that natural gas pipeline leaks may not only lead to fires and explosions, but also cause significant casualties and economic losses. Thus, research on leakage monitoring and early warning technologies for natural gas pipelines is of great significance. In addition, Hu et al.³ established a three-dimensional buried pipeline leakage model to investigate the effects of leak orifice characteristics, pipeline burial depth, and soil conditions on leak diffusion, emphasizing the importance of leakage monitoring. Against this background, Zhang et al.⁴ studied the diffusion mechanisms of hydrogen leakage in buried pipelines, noting that soil corrosion and hydrogen embrittlement are the main factors leading to hydrogen pipeline failure. Understanding the evolution of hydrogen leakage diffusion can facilitate the rapid localization of leakage points and minimize losses.

In the context of the green development of natural gas, hydrogen blending technology has gradually attracted increasing attention. Although the use of hydrogen-blended natural gas can reduce carbon emissions, the safety risks potentially introduced by blending—due to the differences in the physical and chemical properties of hydrogen and natural gas—have not yet been fully clarified. Wang et al.⁵ pointed out that the leakage characteristics of hydrogen-blended natural gas differ significantly from those of conventional natural gas. Therefore, a comprehensive understanding of its safety throughout all stages is essential prior to large-scale application, in order to ensure the healthy development of the industry. Li et al.⁶ further discussed the safety issues associated with long-distance pipeline transportation of hydrogen-blended natural gas, emphasizing the importance of key technologies such as transportation processes, pipeline material compatibility, leakage monitoring, and risk assessment.

¹Shandong Institute of Petroleum and Chemical Technology, Dongying 257061, Shandong, China. ²Efficient Exploration and Development of Oil and Gas Reservoirs and the Integration of Geology and Engineering Shandong Provincial Engineering Research Center, Dongying 257061, Shandong, China. ✉email: 2018010@sdiptc.edu.cn

To address the risks associated with natural gas pipeline leakage, Yan et al.⁷ developed a leakage calculation model based on transient flow equations and the orifice outflow principle, which can effectively describe the leakage process in gas pipelines and provide a reliable method for calculating both leakage rate and cumulative leakage volume. In addition, Feng et al.⁸ investigated the disaster chain characteristics of urban gas pipeline leaks based on Markov chain theory, evaluated pipeline operating conditions, and quantified the failure probability of leakage, thereby providing a basis for cause diagnosis and trend prediction of leakage accidents.

With the deepening of research, the establishment of effective leakage monitoring and early warning systems will help reduce the frequency of leakage incidents and minimize the resulting environmental pollution and economic losses. Zhang et al.⁹ studied the leakage diffusion characteristics of buried natural gas pipelines using a three-dimensional numerical model, highlighting the necessity of leakage monitoring and early warning systems to mitigate potential risks in urban environments. Meanwhile, Zhu et al.¹⁰ conducted experimental studies on the leakage behavior of buried hydrogen and natural gas mixtures, providing important information on leakage diffusion behavior and concentration distribution, which serves as a basis for subsequent safety assessments. Furthermore, Liu et al.¹¹ proposed a Bayesian network-based probabilistic simulation method for leakage orifice diameter, offering a precise approach for estimating leakage rates. Simultaneously, Ndalila et al.¹² utilized computational fluid dynamics software to model the dynamic pressure fluctuation characteristics of gases, revealing the influence of the number and size of leakage orifices on pipeline dynamic pressure. Finally, Li et al.¹³ proposed a novel noise-pressure interaction model, which enhances the accuracy of leakage detection and reduces the likelihood of false alarms.

Yan et al.¹⁴ established a buried gas pipeline leakage model based on the Darcy equation and the mass balance equation. This model takes into account the gas equation of state and can effectively simulate the diffusion process of gas in soil. The geometry of the model is a soil cylinder with the leakage point located within the pipeline. By utilizing axial symmetry, the three-dimensional problem is simplified into a two-dimensional mathematical problem, facilitating analysis and computation. The study by Chang et al.¹⁵ demonstrated that pipeline leakage affects the temperature field of the surrounding soil, and temperature variations in turn influence the diffusion characteristics of the gas. In particular, after a leakage occurs, the temperature gradient in the surrounding soil is significantly affected, which provides a new approach for monitoring. Duan et al.¹⁶ investigated the diffusion characteristics of hydrogen-blended natural gas leakage in utility tunnels and found that the leakage orifice diameter and the orientation of the leakage port significantly affect the spatiotemporal distribution of the combustible gas volume fraction. The larger the leakage orifice, the higher the risk associated with hydrogen leakage; therefore, the characteristics of the leakage port should be considered in pipeline design to reduce potential risks. According to Wu et al.¹⁷, the establishment of leakage location and emission functions provides a theoretical basis for leakage detection, and these theories and methods are also applicable to the daily operation of oil and gas pipelines. Through quantitative analysis of leakage flow rate in relation to pipeline pressure and leakage orifice diameter, important theoretical support can be provided for the safe operation of pipelines. Furthermore, Wang et al.¹⁸ improved the non-adiabatic pipeline leakage model, analyzed the flow characteristics of hydrogen-blended natural gas leakage, and pointed out that the initial pressure and hydrogen blending ratio have significant effects on the leakage flow rate, providing new perspectives for understanding leakage characteristics. Nourollahi et al.¹⁹ proposed an improved one-dimensional characteristic model to simulate the gas leakage process in pipelines and investigated the effects of different boundary conditions on gas emission characteristics, thus offering new theoretical support for leakage detection.

The types of buried pipeline leakage mainly include small-hole leakage and large-hole leakage, which exhibit significant differences in leakage characteristics and impacts. According to Wang et al.⁵, small-hole leakage is typically difficult to detect and can result in significant pressure loss and fluid loss at the time of occurrence. In contrast, large-hole leakage is easier to identify and has a more direct and pronounced impact on the environment. Li et al.⁶ pointed out that leakage from buried pipelines not only causes environmental pollution but may also lead to serious safety accidents. Therefore, effective monitoring and management of different types of leakage are particularly important. In addition, the study by Xu et al.²⁰ emphasized the difficulty in detecting small-hole leaks and proposed an acoustic signal-based detection method that can effectively identify small gas leaks and avoid false alarms caused by traditional detection methods. Li²¹ noted that the mixing of ethanol into hydrogen can accelerate the leakage rate and increase safety risks, which also suggests that leakage characteristics may vary across different gas mixtures.

Soil particle characteristics and soil moisture content play significant roles in the diffusion of hydrogen and hydrogen-blended natural gas leaks. According to Zhao et al.²², the morphology and distribution of soil particles influence the diffusion characteristics of gases within soil, and, in particular, soil moisture has a notable impact on the propagation properties of acoustic waves during the leakage process. The study found that as soil moisture increases, the amplitude and energy of acoustic waves change, and the dominant frequency response of the acoustic signal also varies under different moisture conditions. Yang et al.²³ further explored the effects of buried oil pipeline leakage on the porosity and water saturation of surrounding soil, emphasizing the importance of soil properties in leakage monitoring. Yongmei et al.²⁴ proposed an improved variational mode decomposition method for multi-point leak source detection in urban gas pipelines, highlighting the influence of soil properties on leakage localization accuracy and providing a novel approach to enhance the effectiveness of leak detection. Wang et al.²⁵ introduced a pipeline digital twin model based on pressure signals, which can effectively identify pipeline leaks and trigger emergency responses by updating the data in the physical information space in real time. This approach not only improves the accuracy of leak detection but also offers new perspectives for pipeline management.

Liang et al.²⁶ proposed a pipeline leakage detection method based on acoustic signals, emphasizing that acoustic signals carry physical information about leaks within a short delay period and can be effectively used for pipeline leak diagnosis and localization. This method provides a new direction for leakage monitoring technology,

especially in long-distance pipelines, by collecting vibration signals induced by the acoustic field, thus enhancing the detection capability for small leaks. In addition, the leakage dataset constructed by Xi et al.²⁷ supports the application of deep learning algorithms in natural gas pipeline leak monitoring, achieving a maximum classification accuracy of 95.5% and demonstrating the potential of deep learning in leak detection. Yu et al.²⁸ proposed a novel pipeline leakage detection method based on micro-fiber sensors, which can effectively detect the acoustic signals from small leakage orifices, showing promising application prospects. The pressure gradient detection method based on SCADA systems, proposed by Han²⁹, performed well in simulations; however, real-time data acquisition and processing remain challenging in practical applications. Bin et al.³⁰ detected pipeline anomalies using an active acoustic excitation method, and while experimental results showed high accuracy, the applicability of this approach in complex environments requires further validation. Although some studies have experimentally validated the effectiveness of theoretical models, most still lack support from large-scale field experimental data, which limits the generalizability and application scope of the results. For example, the small-hole leakage experiments conducted by Zhenyi et al.³¹ provided a theoretical foundation for subsequent technology development, but the limitations of experimental conditions may affect the generalizability of the findings.

Despite the extensive research on gas leakage diffusion in soil and atmosphere, studies focusing on the small-hole leakage characteristics of buried pure hydrogen and hydrogen-blended natural gas pipelines remain insufficient. First, existing studies often concentrate on the leakage diffusion characteristics of single-component hydrogen in open spaces, while systematic investigations on the multiphase migration patterns and coupling mechanisms of hydrogen-blended gases leaking from buried pipelines are relatively scarce. Second, current research primarily addresses the leakage diffusion mechanisms of single-component gases in buried pipelines, with limited systematic exploration—especially through experimental and numerical simulation approaches—of the diffusion behavior of hydrogen-blended natural gas at different underground leakage points. To fill these research gaps, this study will conduct an in-depth investigation into the small-hole leakage diffusion of buried pure hydrogen and hydrogen-blended natural gas pipelines. A three-dimensional numerical model for small-hole leakage in buried pipelines will be constructed, with appropriate mesh generation and model independence verification to ensure that the selected model accurately reflects actual conditions. Furthermore, the quantitative effects of leakage orifice characteristics, pipeline burial depth, soil properties, pipeline pressure, and hydrogen blending ratio on leakage rate and diffusion range will be analyzed.

Model description

Geometric model

As shown in Fig. 1, a pipeline model with an outer diameter of 300 mm and a wall thickness of 10 mm was constructed using three-dimensional modeling software. The dimensions of the soil domain are 4 m (length) × 4 m (width) × 2 m (height). A circular leakage hole with a diameter of 5 mm is located at the midpoint of the pipeline. According to the literature, factors such as leakage orifice diameter, leakage direction, pipeline burial depth, soil medium properties, internal pipeline pressure, hydrogen blending ratio, and the shape of the leakage orifice have significant effects on leakage diffusion. Based on this, 23 different leakage scenarios were designed, with specific parameters listed in Tables 1 and 2.

The geometric model was meshed using a structured meshing method. An O-type mesh was applied inside the pipeline, and local mesh refinement was carried out around the leakage orifice. The mesh density gradually decreased from the leakage center towards the periphery, as shown in Fig. 2.

Mesh independence test

During the simulation process, the VOF multiphase flow model, species transport model, and k- ϵ turbulence model were adopted. The numerical model used a pressure-velocity coupling approach with the SIMPLE algorithm. The momentum equation was spatially discretized using the Second Order Upwind scheme, the

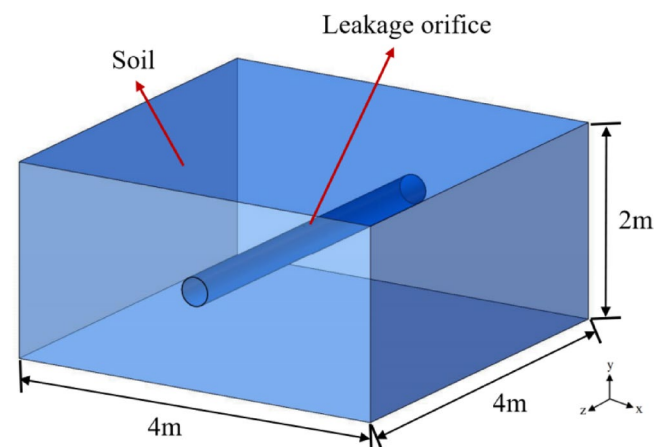


Fig. 1. Geometric model of buried pipeline leakage.

Serial Number	Outer Diameter/mm	Leakage Orifice Shape	Leakage Orifice Diameter / mm	Leakage Orifice Orientation	Burial Depth/m	Soil Type	Pressure/MPa	Hydrogen Blending Ratio/%	Sensitivity Factor
1	300	Circular	5	Upward	1	A	0.5	100	Leakage Orifice Diameter
2	300	Circular	3	upward	1	A	0.5	100	
3	300	circular	7	Upward	1	A	0.5	100	
4	300	Circular	10	Upward	1	A	0.5	100	
5	300	Circular	5	Downward	1	A	0.5	100	Leakage Orifice Orientation
6	300	circular	5	Upward	0.8	A	0.5	100	Burial Depth
7	300	circular	5	Upward	1.2	A	0.5	100	
8	300	Circular	5	Upward	1.4	A	0.5	100	
9	300	Circular	5	Upward	1	B	0.5	100	Soil Type
10	300	Circular	5	Upward	1	C	0.5	100	
11	300	Circular	5	Upward	1	D	0.5	100	
12	300	Circular	5	Upward	1	E	0.5	100	
13	300	circular	5	upward	1	A	0.3	100	Pressure
14	300	Circular	5	Upward	1	A	0.8	100	
15	300	Circular	5	Upward	1	A	1	100	
16	300	Circular	5	Upward	1	A	1.5	100	
17	300	Circular	5	Upward	1	A	0.5	80	Hydrogen Blending Ratio
18	300	Circular	5	Upward	1	A	0.5	60	
19	300	Circular	5	Upward	1	A	0.5	40	
20	300	circular	5	Upward	1	A	0.5	20	
21	300	Circular	5	Upward	1	A	0.5	0	
22	300	Radial rectangular slit	1 × 19.625	Upward	1	A	0.5	100	Leakage Orifice Shape
23	300	Axial rectangular slit	19.625 × 1	Upward	1	A	0.5	100	

Table 1. Simulation Conditions.

Soil Type	Soil Particle Size/mm	Porosity	Viscous Resistance Coefficient/m ⁻²	Inertial Resistance Coefficient/m ⁻¹
A	0.05	0.43	2.45×10^{11}	501,842
B	0.1	0.43	6.13×10^{10}	250,921
C	0.01	0.43	6.13×10^{12}	2,509,213
D	0.05	0.3	1.09×10^{12}	1,814,815
E	0.05	0.55	7.30×10^{10}	189,331

Table 2. Soil Parameters.

pressure was discretized using the PRESTO! method, and the volume fraction was discretized using the Geo-Reconstruct method. The time step was set to 10^{-4} s, and the maximum number of iterations was set to 200.

By setting different maximum mesh sizes, mesh models with 403,742; 864,365; 1,068,143; and 1,309,748 cells were generated. Under operating condition 1, the time-history curves of hydrogen volume fraction at the monitoring point 0.35 m directly above the leakage orifice were obtained for different mesh densities, as shown in Fig. 3. It can be seen from the figure that when the mesh number increased from 1,068,143 to 1,309,748, the deviation of hydrogen volume fraction at the monitoring point was less than 1%. Therefore, to ensure calculation accuracy and improve computational efficiency, the mesh with 1,068,143 cells was selected for numerical simulation.

Governing equations and Boundary/Initial conditions

Governing equations The leakage and diffusion process is modeled using the continuity equation, momentum equation, and species transport equation, along with the standard k- ϵ turbulence model and VOF multiphase model. The gas transport through the soil (porous medium) is modeled by incorporating a Darcy-Forchheimer source term into the momentum equations, characterized by the viscous and inertial resistance coefficients detailed in Table 2. The Ideal Gas Law is assumed to apply due to the low operating pressure range of the distribution pipeline (≤ 1.5 MPa).

Boundary Conditions (BCs):

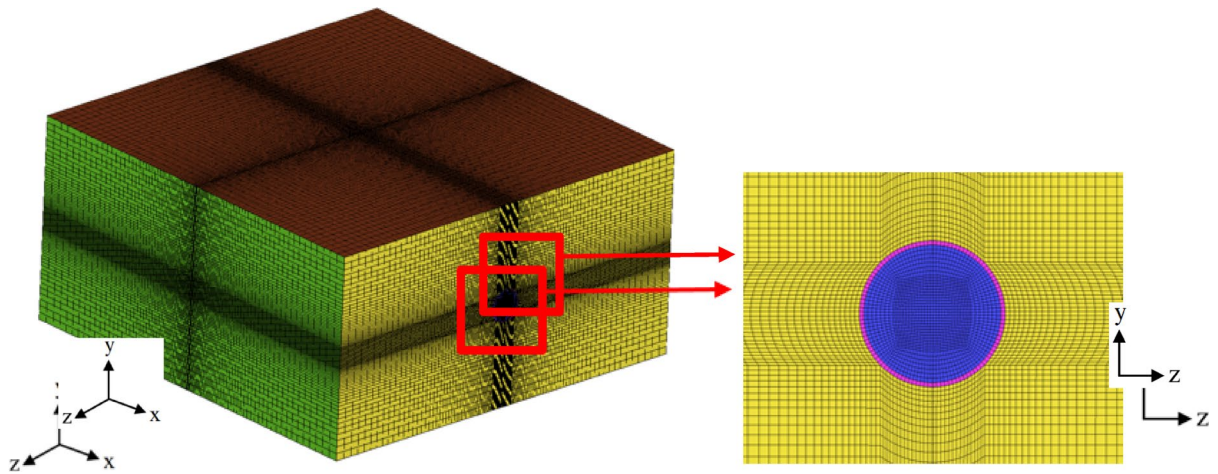


Fig. 2. The grid model for three dimensional numerical simulation.

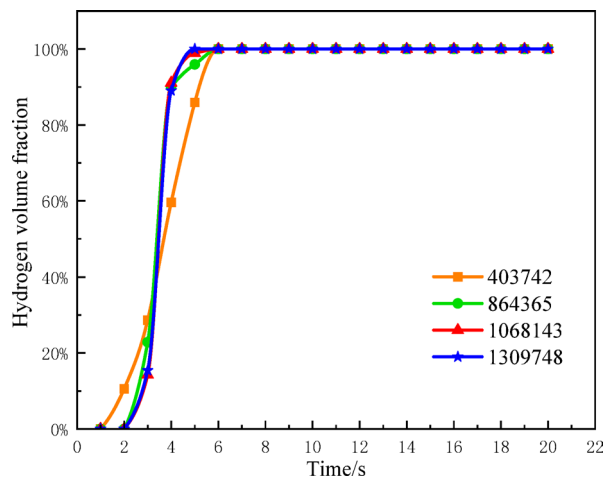


Fig. 3. Distribution curves of hydrogen volume fraction at the monitoring point 0.35 m directly above the leakage orifice within 20 s of leakage.

Leakage Orifice: Defined as a Pressure-Inlet boundary, specifying the static pressure and 293.15 K temperature corresponding to the pipeline operating conditions (Table 1).

Soil Domain Side Walls and Bottom: Defined as Impermeable Walls (Neumann boundary condition: zero-gradient for concentration, $\partial C/\partial n = 0$).

Ground Surface (Top Boundary, $y=2$ m): Defined as an Atmospheric Outlet/Pressure-Outlet boundary, allowing gas to escape freely into the atmosphere and maintaining atmospheric pressure (101.325 kPa).

Pipeline Wall (Inner and Outer): Defined as non-slip walls.

Initial Conditions (ICs):

Soil Domain: Initially, the entire soil domain is filled with air at rest. The hydrogen volume fraction is set to 0 throughout the soil. The pressure is initialized to the atmospheric pressure (101.325 kPa), and the temperature is 293.15 K.

Model validation

To ensure the robustness and reliability of our numerical simulation method, particularly concerning the leakage dynamics that define the boundary condition input, we performed a quantitative validation of the calculated gas mass flow rate. We compared the transient mass flow rate predicted by our CFD model's pressure-inlet setup with an established theoretical model for transient gas leakage, specifically the one based on the Van der Waals Equation of State (VDW-EOS) (Zhou et al., 2018, DOI:<https://doi.org/10.1016/j.ijhydene.2018.04.141>).

For the reference case (Condition 1: $D=5$ mm, $P=0.5$ MPa), the CFD model predicted an initial mass flow rate of $q_{m,CFD}=0.0385$ kg/s. The VDW-EOS model for the same conditions predicted $q_{m,VDW-EOS}=0.0366$ kg/s. The relative deviation between the two models is approximately 5.2%. This small deviation, which is consistent with industry standards, validates the robustness and accuracy of the pressure-inlet boundary condition used in our numerical simulations for predicting the leakage rate.

Code Availability

The custom code used for the numerical simulations in this study has been developed based on the commercial Computational Fluid Dynamics (CFD) software [ANSYS FLUENT 2021 R2] using its standard solvers (VOF multiphase, species transport, and $k-\epsilon$ turbulence models). No unique custom source code or mathematical algorithm requiring separate public deposition was written to generate the final results.

Numerical results

Leakage orifice diameter D

To investigate the influence of leakage orifice diameter on the diffusion of hydrogen leakage from buried pure hydrogen pipelines, numerical simulations were carried out for leakage orifice diameters of 3 mm, 5 mm, 7 mm, and 10 mm.

Using the aforementioned numerical model, hydrogen volume fraction distribution contour plots along the radial direction of the leakage orifice at 80 s after leakage were obtained for different orifice diameters, as shown in Fig. 4. It can be observed from the figure that the leakage exhibits a circular diffusion pattern, with higher hydrogen volume fractions closer to the orifice, reaching up to 100% around the leakage hole. When the orifice diameter is 3 mm (Fig. 4a), the diffusion area is relatively small, and hydrogen is concentrated near the leakage orifice. As the orifice diameter increases (Fig. 4b and c), the diffusion area further expands, and the edge of the high-concentration region shows a regular arc shape. When the orifice diameter increases to 10 mm, the diffusion area expands further, and with the increase of diffusion distance, the edge of the high-concentration region becomes irregular.

As shown in Fig. 5, a monitoring point is located 0.35 m vertically above the leakage orifice, where the time-history curves of hydrogen volume fraction at the monitoring point under different leakage orifice diameters were recorded for the buried pure hydrogen pipeline. The results show that under all orifice diameter conditions, the hydrogen volume fraction at the monitoring point eventually reaches a saturated state. However, the time required to reach the maximum concentration decreases significantly with the increase of the leakage orifice diameter: when the orifice diameter is 3 mm, it takes 200 s for the monitoring point to reach the maximum concentration; for an orifice diameter of 5 mm, the time is reduced to 130 s; for 7 mm, only 120 s is needed; and for 10 mm, the time further decreases to 80 s. Further analysis of the trend of the curves reveals that as the leakage orifice diameter increases, the slope of the hydrogen volume fraction rise stage becomes steeper, indicating a significantly faster accumulation rate of hydrogen at the monitoring point. This is because the increase in orifice diameter directly enhances the fluid velocity and the amount of hydrogen leakage at the orifice. A larger orifice provides a wider passage for hydrogen escape, allowing more hydrogen to enter the soil through the leakage orifice and diffuse to the monitoring point in a shorter time, thus accelerating the accumulation of hydrogen concentration. In addition, the larger the orifice diameter, the greater the total amount of hydrogen escaping into the soil per unit time, resulting in a significantly higher overall hydrogen volume fraction in the diffusion region. Therefore, the leakage orifice diameter not only affects the rate at which hydrogen at the monitoring point reaches saturation, but also significantly increases the hydrogen concentration level and diffusion risk in the soil.

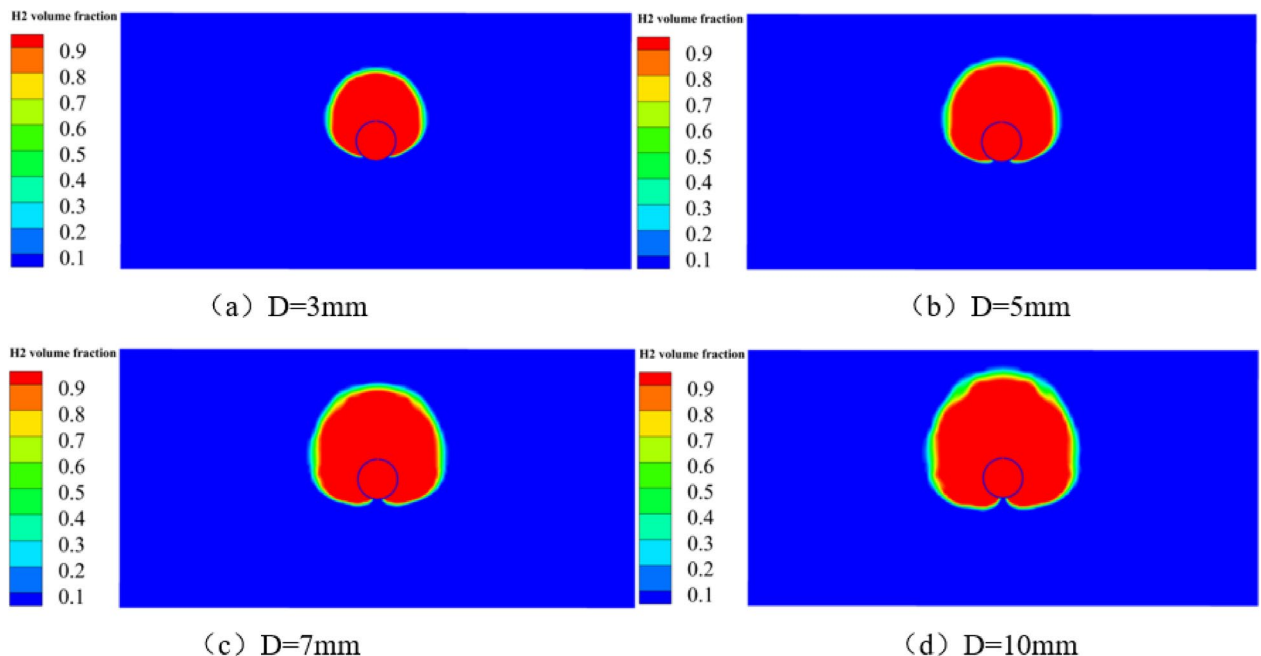


Fig. 4. Hydrogen volume fraction distribution contours along the radial direction of the leakage orifice at 80 s for different leakage orifice diameters.

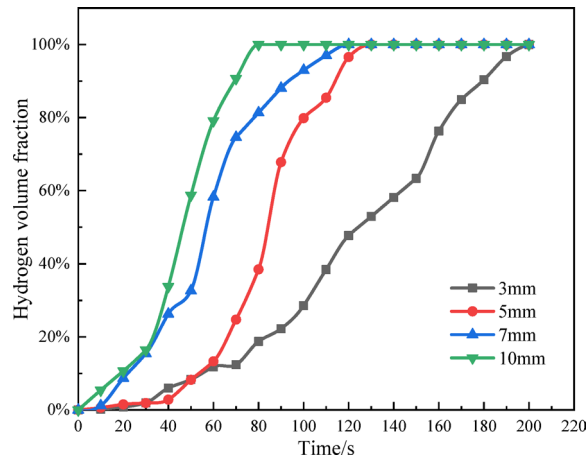


Fig. 5. Variation curves of hydrogen volume fraction at the monitoring point under different leakage orifice diameters.

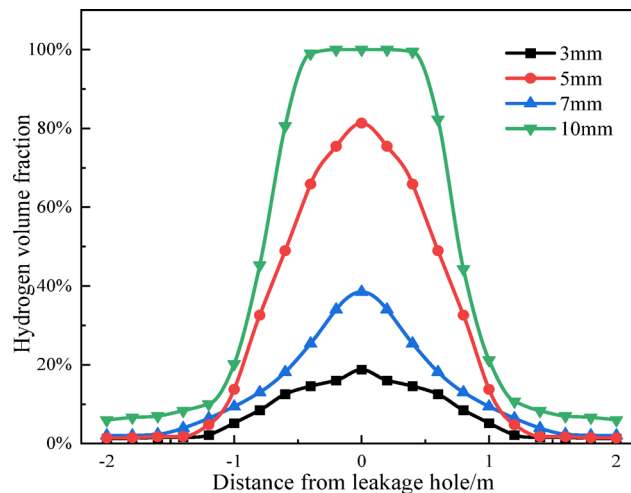


Fig. 6. Hydrogen volume fraction distribution along the axial direction at the monitoring point after 80 s of leakage under different leakage orifice diameters.

Figure 6 shows the distribution curves of hydrogen volume fraction along the axial direction of the leakage orifice at the monitoring point after 80 s of leakage under different orifice diameters for the buried pure hydrogen pipeline. As can be observed from the figure, under the same orifice diameter, the hydrogen volume fraction exhibits a symmetric distribution. For different orifice diameters, the hydrogen volume fraction displays a clear gradient distribution, and the peak value of each curve is located at the monitoring point directly above the leakage orifice.

With the increase of leakage orifice diameter, the peak value of the curve gradually rises. When the orifice diameter is 10 mm, the peak reaches 100%; for an orifice diameter of 5 mm, the peak is 81.3%; for 7 mm and 3 mm, the peak values are 38.5% and 18.8%, respectively. It is worth noting that at positions far from the leakage point (± 2 m), the hydrogen volume fractions corresponding to all curves are close to 5%, indicating that the impact of leakage diffusion at these locations is relatively weak.

Leakage orifice orientation

As shown in Fig. 7, by adjusting the direction of the leakage orifice to be either vertically upward or downward, the model was used to simulate the distribution of hydrogen volume fraction along the radial direction of the leakage orifice after 200 s of leakage in a buried pure hydrogen pipeline. The contour plots clearly reflect the significant influence of leakage orifice orientation on hydrogen diffusion behavior. When the leakage orifice faces upward, due to the much lower density of hydrogen compared to air, the leaked hydrogen rapidly diffuses upward along the vertical direction. In this case, a high-concentration hydrogen region quickly forms above the leakage point, and hydrogen continues to diffuse both upward and outward, resulting in a larger diffusion range. This is because the lightweight property of hydrogen allows it to overcome soil resistance more easily when leaking upward, enabling it to migrate more quickly to the surface or even higher, thus exhibiting a pronounced upward

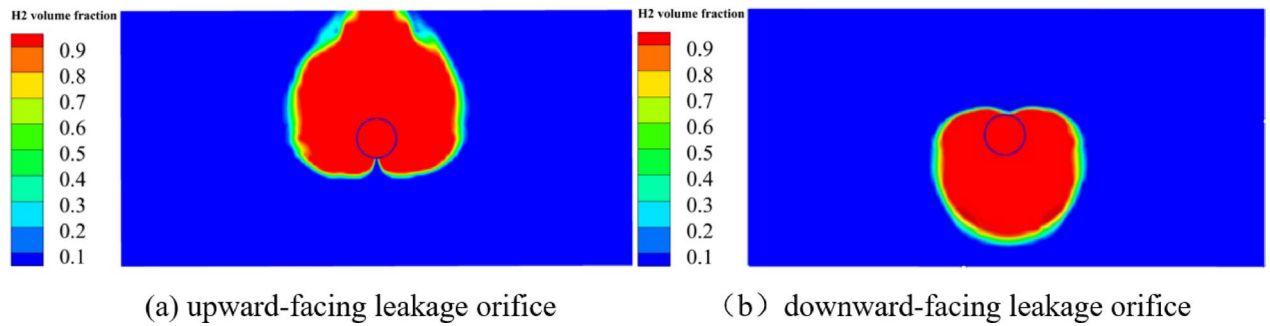


Fig. 7. Radial hydrogen volume fraction contours at 200 s for different orientations of the leakage orifice.

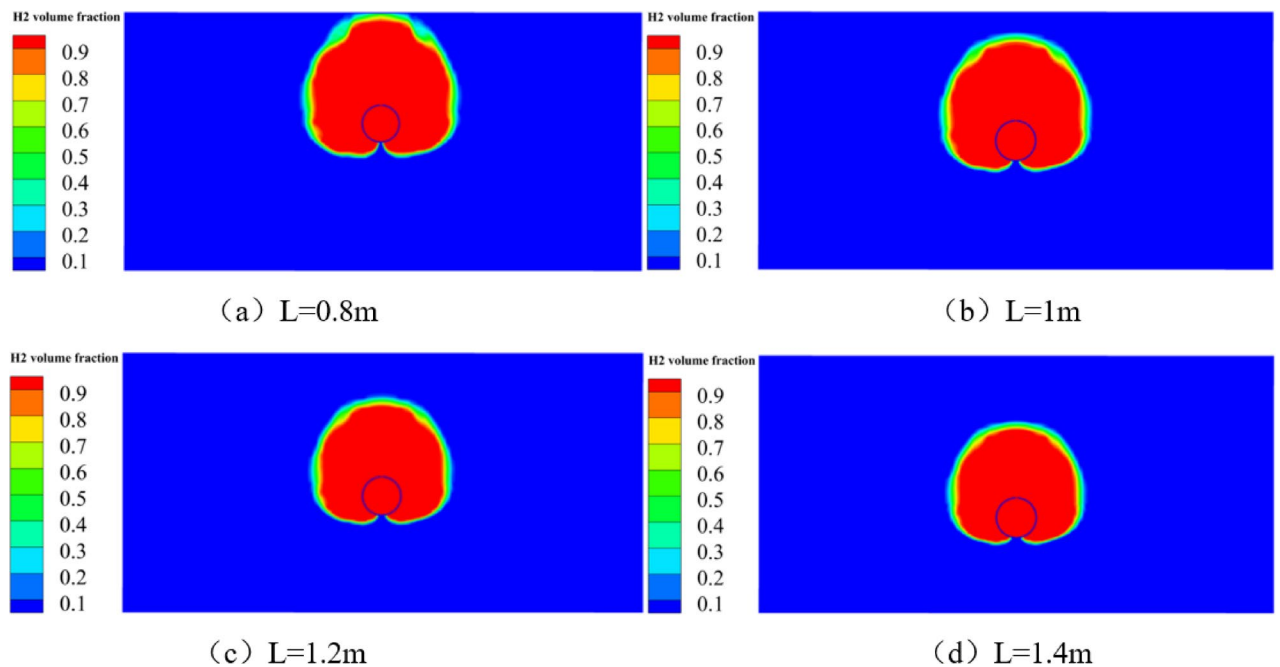


Fig. 8. Radial hydrogen volume fraction contours at 120 s after leakage for different pipeline burial depths.

and outward diffusion trend. In contrast, when the leakage orifice faces downward, hydrogen is initially forced to diffuse downward, forming a high-concentration region below the leakage point for a short period. However, due to its low density, hydrogen will gradually rise over time and eventually diffuse upward. During this process, hydrogen must first overcome soil resistance and the effect of gravity, resulting in a slower diffusion speed and a shorter existence time for the high-concentration region below. Ultimately, hydrogen will still accumulate and rise to the area above the leakage point. In summary, the orientation of the leakage orifice significantly affects the diffusion path and rate of hydrogen in the soil. When leaking upward, hydrogen can rapidly rise and diffuse with the help of its low density, forming a larger high-concentration region. When leaking downward, the diffusion path is somewhat hindered, with hydrogen initially accumulating below but eventually migrating upward due to density differences.

Burial depth L

To investigate the influence of pipeline burial depth on leakage diffusion, the diffusion processes were simulated for burial depths of 0.8 m, 1 m, 1.2 m, and 1.4 m. Using the aforementioned model, hydrogen volume fraction distribution contour plots along the radial direction of the leakage orifice at 120 s after leakage were obtained, as shown in Fig. 8. It can be seen from the figure that at 120 s, the contour plots exhibit an approximately symmetrical distribution. As the burial depth increases, the diffusion range of hydrogen within the soil layer gradually decreases. When the pipeline is buried at a depth of 0.8 m (Fig. 8a), the edge of the high-concentration diffusion region displays an irregular pattern, and the diffusion distance directly above the leakage orifice is the greatest, with hydrogen already diffusing to the top of the soil layer, although the concentration is not high. When the burial depth increases to 1.4 m (Fig. 8d), the diffusion range of hydrogen is significantly reduced, and

the boundary of the high-concentration region appears as a smooth curved surface. This is because a greater burial depth results in higher soil pressure, thus further restricting the diffusion range of the leaked hydrogen.

As shown in Fig. 9, the hydrogen volume fraction at a monitoring point located 0.35 m vertically above the leakage orifice was recorded for buried pure hydrogen pipelines at different burial depths during the leakage process. The curves show the variation of hydrogen volume fraction at the monitoring point over time under different burial depths. It can be seen that the overall diffusion pattern of hydrogen leakage is generally consistent under various burial depths: in the initial stage (0–60 s), each curve rises slowly; between 60 s and 100 s, the hydrogen volume fraction at the monitoring point increases rapidly, quickly reaching around 80%; from 100 s to 120 s, the growth rate slows down significantly, gradually approaching saturation; after 120 s, all curves level off, and the hydrogen volume fraction ultimately stabilizes at 100%. Further comparison of the diffusion processes under different burial depths shows that, at the same leakage time, the hydrogen volume fraction at the monitoring point decreases as the burial depth increases. For example, at 100 s, the hydrogen concentration for a burial depth of 1.4 m is 10.83% lower than that for 0.8 m. This indicates that the greater the burial depth, the longer the diffusion path for hydrogen from the leakage point to the monitoring point, and the more significant the hindering effect of the soil on the gas, resulting in a slower arrival of hydrogen at the monitoring point and a reduced accumulation rate of concentration. This is because a larger burial depth means a longer diffusion distance for hydrogen in the soil, with increased soil resistance and adsorption during the diffusion process, which restricts gas migration and slows the rate of concentration increase at the monitoring point, thus extending the time required to reach saturation. Conversely, when the burial depth is shallower, the diffusion path is shorter and the resistance is smaller, allowing hydrogen to reach and accumulate at the monitoring point more quickly.

The distribution curves of hydrogen volume fraction along the axial direction of the leakage orifice at the monitoring point for buried pure hydrogen pipelines after 120 s of leakage under different burial depths are shown in Fig. 10. As can be seen from the figure, hydrogen diffuses symmetrically on both sides of the leakage point. The hydrogen volume fraction reaches its maximum at the monitoring point directly above the leakage orifice, with values of 98.6%, 96.6%, 93.5%, and 90.6% for burial depths of 0.8 m, 1.0 m, 1.2 m, and 1.4 m, respectively. The hydrogen volume fraction for a burial depth of 0.8 m is 1.02 times that at 1.0 m, 1.05 times that at 1.2 m, and 1.09 times that at 1.4 m. When the burial depth is 0.8 m, the hydrogen volume fraction at the monitoring point changes more rapidly, and the curve is similar to those of other burial depths, indicating that burial depth has a certain influence on the hydrogen volume fraction, but its effect is relatively small compared to other influencing factors. In general, the shallower the burial depth, the higher the hydrogen concentration at the monitoring point and the larger the diffusion range.

Soil type

Different soil environmental conditions significantly affect the diffusion behavior of hydrogen in soil after leakage from buried hydrogen pipelines. In particular, differences in soil particle size and porosity directly influence the viscous and inertial resistance coefficients of the soil, thereby determining the diffusion characteristics of gas in the soil. By adjusting the soil porosity to 0.43, 0.3, and 0.55, simulations were carried out using the aforementioned model. The hydrogen volume fraction contour plots along the radial direction of the leakage orifice at the monitoring point after 100 s of leakage under three different soil porosity conditions are shown in Fig. 11. As shown in the figure, the hydrogen volume fraction distribution exhibits a symmetrical circular diffusion pattern under different soil porosities. The effect of soil porosity on gas leakage is quite significant. When the soil porosity is 0.3, the hydrogen diffusion region is very small and concentrated near the leakage orifice. When the porosity is 0.43 (Fig. 11a), the hydrogen diffusion range is still relatively small and shows a regular circular shape. When the porosity increases to 0.55 (Fig. 11c), the diffusion range of hydrogen increases substantially, and the region directly above the leakage orifice has already reached the soil surface. The higher

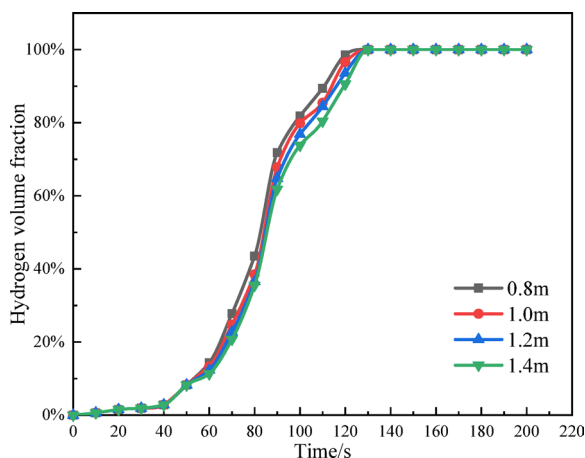


Fig. 9. Time-history curves of hydrogen volume fraction at the monitoring point for different pipeline burial depths.

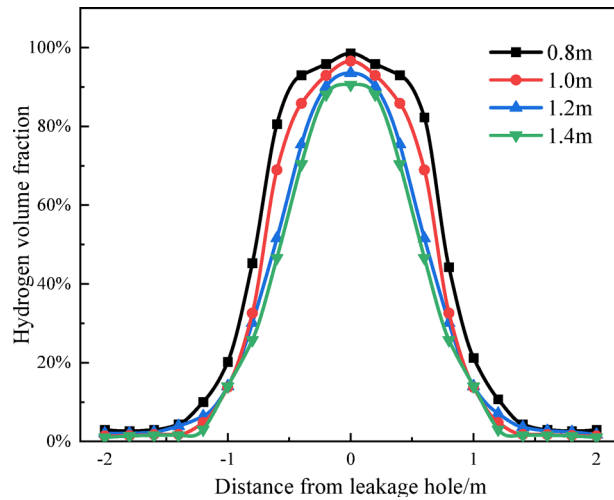


Fig. 10. Axial hydrogen volume fraction distribution curves at the monitoring point after 120 s of leakage for different burial depths.

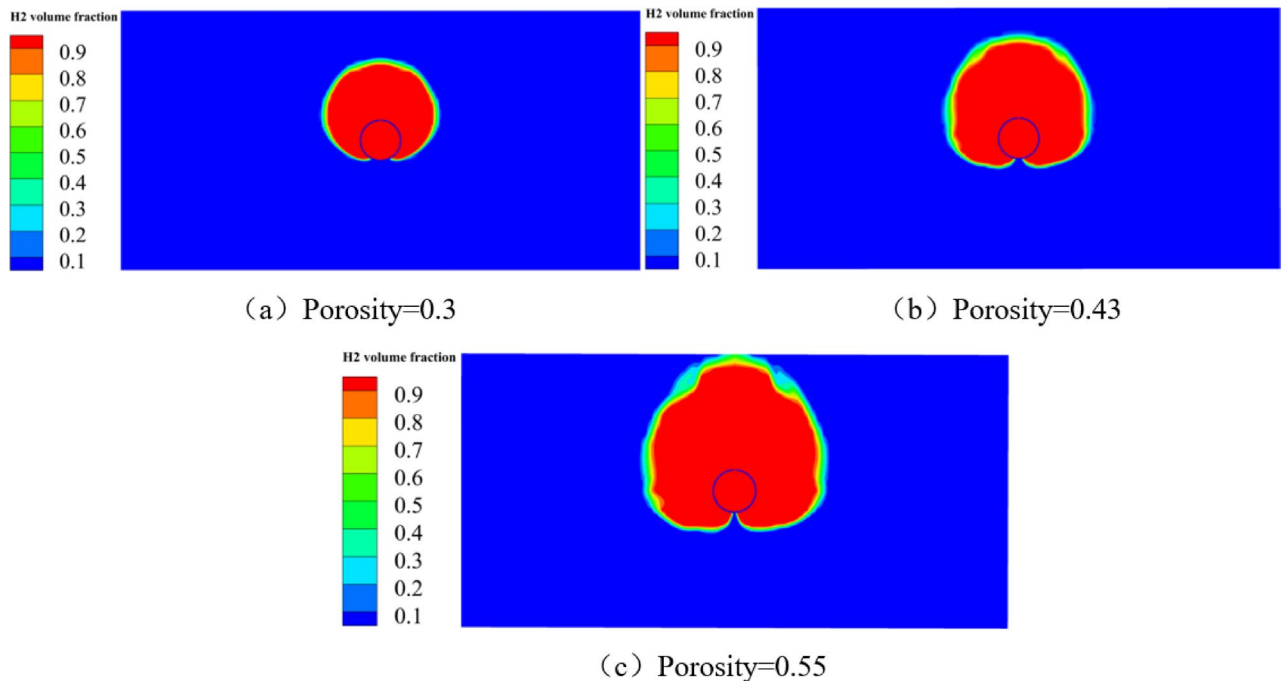


Fig. 11. Radial hydrogen volume fraction distribution contours at 100 s after leakage under different soil porosities.

the porosity, the greater the hydrogen volume fraction and the wider the affected area at the same time; the distribution range of low concentrations also increases.

As shown in Fig. 12, the hydrogen volume fraction at a monitoring point located 0.35 m vertically above the leakage orifice was recorded during the leakage process of buried pure hydrogen pipelines under different soil porosities. The curves in the figure show that, under the same porosity condition, the hydrogen volume fraction increases rapidly over time and stabilizes after reaching saturation. A further comparison of the curves for different porosities reveals that, as the soil porosity increases, the rate at which the hydrogen concentration rises at the monitoring point is significantly accelerated, and the time required to reach saturation is notably shortened: when the porosity is 0.3, the saturation time is 200 s; for a porosity of 0.43, the saturation time is 130 s; and for a porosity of 0.55, it takes only 100 s to reach saturation. This is because higher soil porosity means more void space in the soil, which facilitates gas diffusion and migration. Greater porosity provides more diffusion channels for hydrogen, reduces the resistance encountered by the gas as it migrates through the soil, and allows hydrogen to reach and accumulate at the monitoring point more quickly, thereby significantly

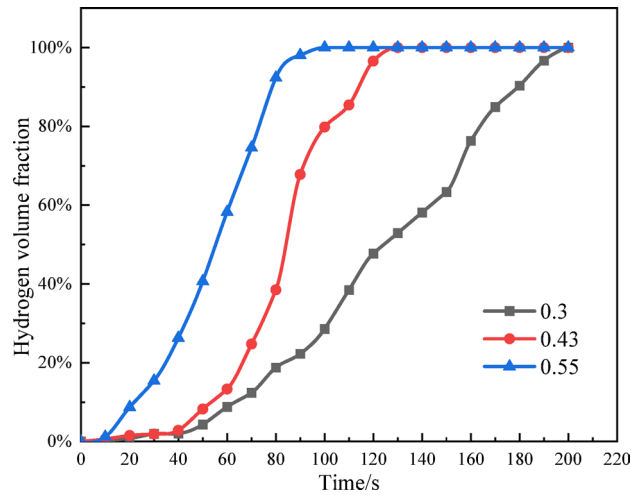


Fig. 12. Variation curves of hydrogen volume fraction versus time at the monitoring point for buried pure hydrogen pipelines under different soil porosities.

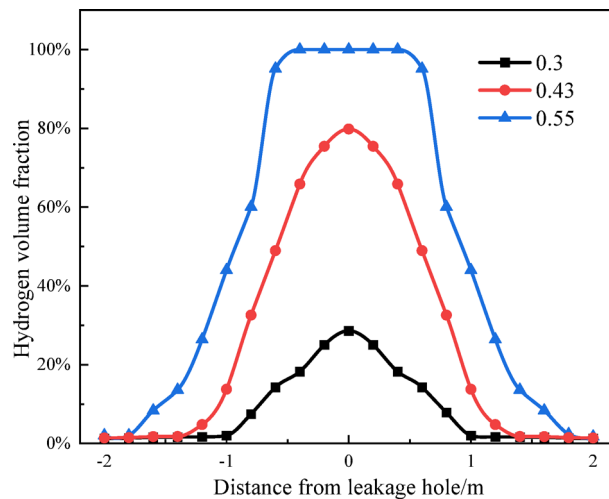


Fig. 13. Axial distribution curves of hydrogen volume fraction at the monitoring point after 100 s of leakage under different soil porosities.

enhancing the diffusion rate and the rate of concentration accumulation. In contrast, when the porosity is lower, the soil structure is denser, gas diffusion is restricted, and it takes longer for hydrogen to reach saturation at the monitoring point.

The distribution curves of hydrogen volume fraction along the axial direction of the leakage orifice at the monitoring point after 100 s of leakage under different soil porosities are shown in Fig. 13. At the same time point, as the soil porosity increases, the peak value of hydrogen concentration at the monitoring point increases, reaching 28.6%, 79.8%, and 100% for porosities of 0.3, 0.43, and 0.55, respectively. This indicates that the higher the soil porosity, the greater the accumulation of hydrogen at the monitoring point. Moving away from the peak, the hydrogen volume fraction gradually decreases on both sides, and the rate of decrease is related to the soil porosity—the higher the porosity, the faster the decrease rate.

Figure 13

The soil particle size was adjusted to 0.05 mm, 0.1 mm, and 0.01 mm, respectively. Simulations were carried out using the above model, and the hydrogen volume fraction contour plots along the radial direction of the leakage orifice at the monitoring point after 100 s of leakage under different soil particle size conditions were obtained, as shown in Fig. 14. It can be observed from the figure that soil particle size has a significant impact on the diffusion of leaked gas. At 100 s after leakage, the smaller the soil particle diameter, the slower the hydrogen diffusion and the smaller the diffusion range. When the soil particle diameter is 0.01 mm (Fig. 13a), hydrogen is mainly concentrated near the leakage orifice, showing a regular circular diffusion pattern. When the soil particle diameter is 0.05 mm, the hydrogen diffusion range increases significantly, and irregular low-concentration

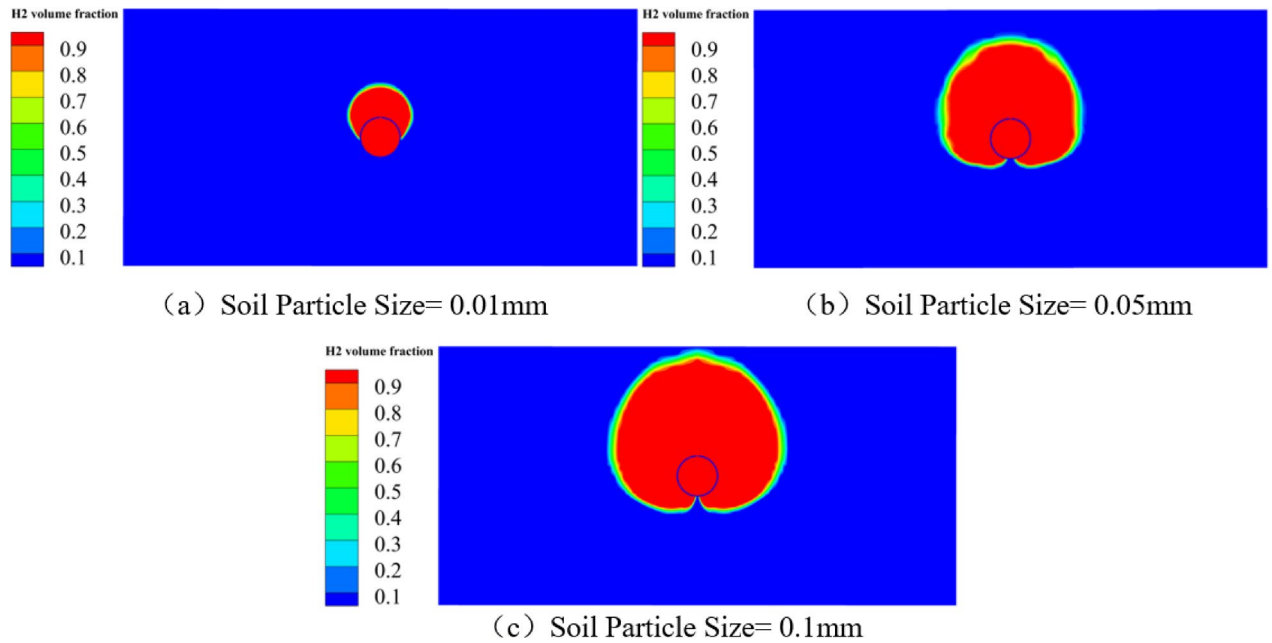


Fig. 14. Radial hydrogen volume fraction distribution contours at 100 s after leakage under different soil particle sizes.

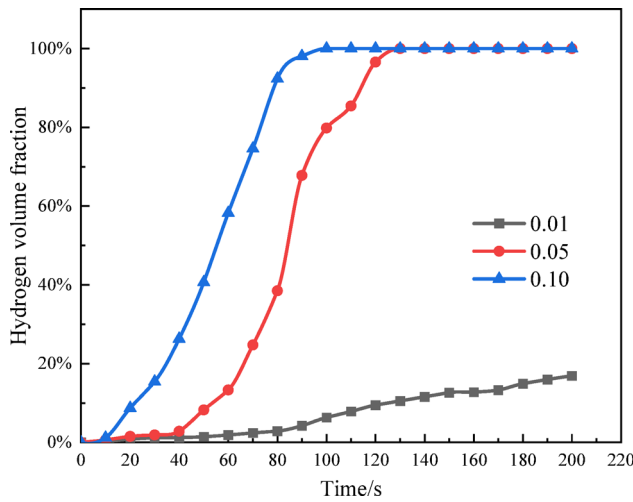


Fig. 15. Variation curves of hydrogen volume fraction versus time at the monitoring point for different soil particle sizes.

regions appear. When the soil particle diameter is 0.1 mm, the diffusion range further expands, and the diffusion region approaches the ground surface.

At a monitoring point located 0.35 m vertically above the leakage orifice, the time-history curve of hydrogen volume fraction at the monitoring point was obtained, as shown in Fig. 15. It can be observed from the figure that soil particle size has a significant effect on the diffusion of leaked gas. When the soil particle size is 0.01 mm, the hydrogen volume fraction at the monitoring point increases very slowly within 200 s, reaching only 16.9% after 200 s of leakage. When the particle size is 0.05 mm, the hydrogen volume fraction at the monitoring point increases more significantly within 200 s compared to the previous case, and approaches saturation at around 130 s. For a particle size of 0.10 mm, the hydrogen volume fraction at the monitoring point changes even more rapidly, reaching saturation at 100 s, and the growth rate is smoother and more stable compared to the other two cases.

Under different soil particle size conditions, the distribution of hydrogen volume fraction along the axial direction of the leakage orifice at the monitoring point after 100 s of leakage from the buried pure hydrogen pipeline is shown in Fig. 16. The results show that when the soil particle size is 0.01 mm, the hydrogen volume fraction at the monitoring point is relatively low, with a peak value of only 6.3%, and the distribution along the

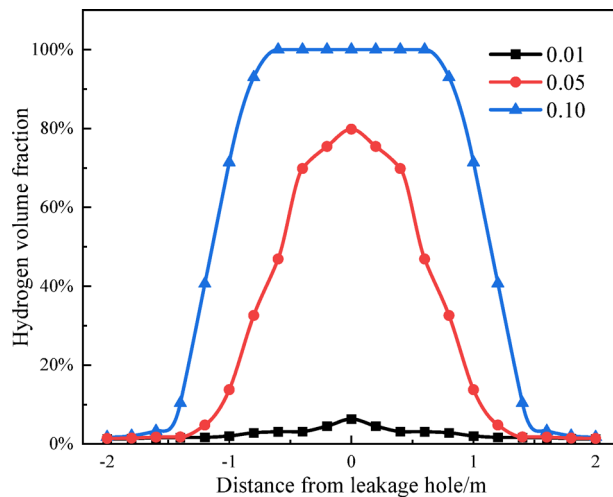


Fig. 16. Axial distribution curves of hydrogen volume fraction at the monitoring point after 100 s of leakage under different soil particle sizes.

pipeline direction is relatively flat, indicating that hydrogen diffuses more slowly in fine-grained soil. When the soil particle size increases to 0.05 mm, the peak hydrogen volume fraction increases significantly to 79.8%, and hydrogen is mainly distributed within the range of -1 m to 1 m, with an expanded affected area, suggesting that medium particle size soil is more conducive to hydrogen diffusion. When the soil particle size further increases to 0.10 mm, the peak hydrogen volume fraction reaches 100%, and maintains a high level near the monitoring point, with a more concentrated distribution, indicating that larger particle size soil can significantly accelerate the diffusion rate of hydrogen. This is because, with smaller soil particle sizes, the pores between soil particles are finer, which impedes the diffusion path of hydrogen in the soil, resulting in a lower diffusion rate, lower hydrogen concentration, and a more uniform distribution. As the soil particle size increases, the soil porosity increases, the resistance to gas molecule movement decreases, and hydrogen can diffuse more easily along the pores, leading to a higher peak volume fraction near the leakage orifice, faster diffusion rate, and a more concentrated distribution range. Therefore, soil particle size is an important factor affecting the diffusion behavior of hydrogen leakage from buried pipelines.

In summary, both soil porosity and particle size have significant effects on the diffusion behavior of hydrogen leakage. As soil porosity increases, the accumulation of hydrogen at the leakage point increases, resulting in a higher peak volume fraction and a faster diffusion rate, which leads to a more concentrated affected area. In soils with larger particle sizes, hydrogen can rapidly reach high concentrations near the leakage point, posing a higher safety risk; whereas in soils with smaller particle sizes, although the hydrogen volume fraction is lower, the diffusion process is slower, which may cause a prolonged impact on the surrounding environment. Overall, the combined effect of larger soil porosity and particle size reduces the soil's resistance coefficient, decreases the resistance to hydrogen diffusion in the soil, thereby accelerating the diffusion rate and expanding the diffusion range. These results indicate that the physical properties of soil are important factors influencing the diffusion and risk of hydrogen leakage from buried pipelines.

Pipeline pressure P

The pipeline pressure was set to 0.3 MPa, 0.5 MPa, 0.8 MPa, 1.0 MPa, and 1.2 MPa, respectively. Based on the established model, simulations of the leakage process of a buried pure hydrogen pipeline under these five different pressure conditions were conducted, and the temporal variation of hydrogen volume fraction at the monitoring point was obtained. Taking 100 s after leakage as a reference point, the radial distribution contour plots of hydrogen volume fraction along the leakage orifice were generated, as shown in Fig. 17. As can be seen from the contour plots, when only the pipeline pressure is changed, the geometric shape of the leaked hydrogen distribution remains relatively stable, with all five pressure conditions showing a symmetrical and approximately circular diffusion pattern. As the pipeline pressure increases, the diffusion-affected area of hydrogen gradually expands, and when the pressure reaches 1.2 MPa, the diffusion range of leaked hydrogen is already close to the ground surface. This is because the increase in pipeline pressure significantly raises the hydrogen flow velocity and leakage rate at the orifice, resulting in a greater amount of hydrogen escaping into the soil per unit time, which in turn drives the hydrogen to diffuse further in the radial direction and expands the affected area. However, since the physical structure and diffusion properties of the soil remain unchanged, the geometric shape of hydrogen diffusion maintains its symmetry and circular distribution. With further increases in pressure, hydrogen can more easily overcome soil resistance, and the tendency for upward diffusion toward the surface becomes more pronounced, thereby increasing the risk of surface leakage.

At a monitoring point located 0.35 m vertically above the leakage orifice, the time-history curves of hydrogen volume fraction at this point under different pipeline pressures were obtained, as shown in Fig. 18. The results indicate that pipeline pressure has a significant effect on the variation of hydrogen volume fraction during leakage. Overall, the trends of hydrogen volume fraction under the five pressure conditions are generally consistent: in

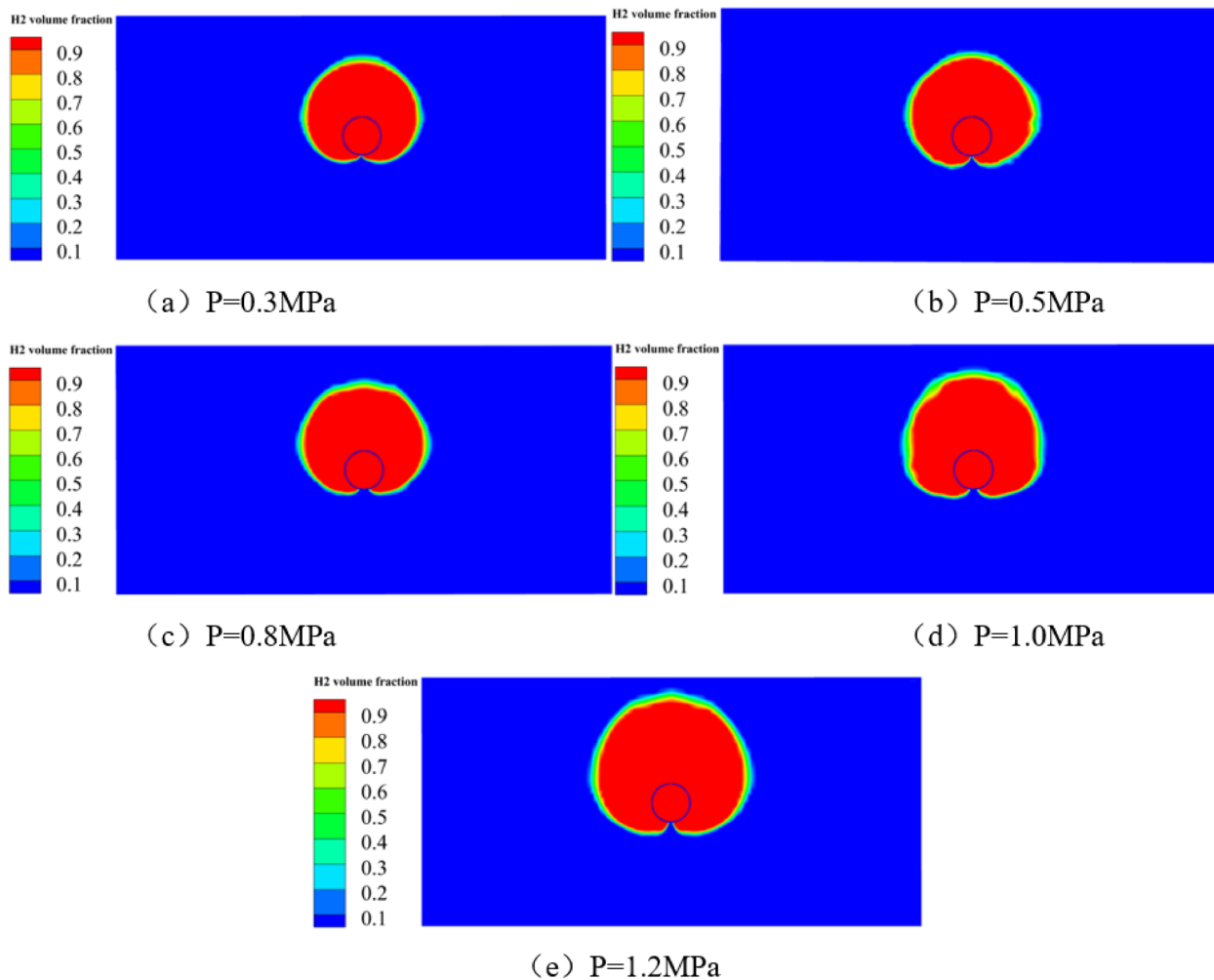


Fig. 17. Radial hydrogen volume fraction distribution contours at 100 s after leakage under different pipeline pressures.

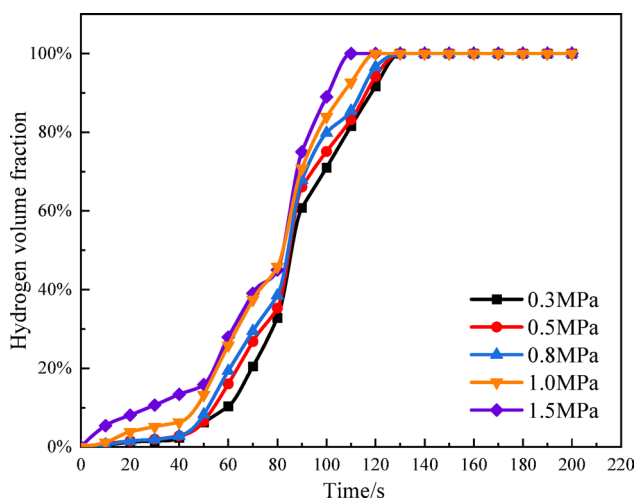


Fig. 18. Variation curves of hydrogen volume fraction versus time at the monitoring point for different pipeline pressures.

the initial stage of leakage (0–40 s), the hydrogen volume fraction at the monitoring point increases relatively slowly; during the 40–80 s stage, the growth rate accelerates noticeably; in the subsequent saturation stage, the hydrogen volume fraction continues to rise rapidly until it stabilizes. Specifically, when the pipeline pressures are 0.3 MPa, 0.5 MPa, and 0.8 MPa, the hydrogen volume fraction at the monitoring point reaches saturation at around 130 s; when the pressure is 1.0 MPa, the saturation time is shortened to about 120 s; and at 1.2 MPa, the monitoring point approaches saturation at approximately 110 s. This is because as the pipeline pressure increases, the hydrogen flow velocity and leakage rate at the orifice also increase, resulting in more hydrogen escaping into the soil per unit time. Consequently, hydrogen reaches the monitoring point more quickly, causing the volume fraction to rise rapidly. In addition, the driving force for leakage is greater at higher pressures, which further increases the diffusion rate of hydrogen in the soil, thereby reducing the time required to reach saturation. In summary, the higher the pipeline pressure, the faster the accumulation of hydrogen at the monitoring point and the shorter the saturation time, demonstrating the accelerating effect of pipeline pressure on the hydrogen leakage diffusion process.

As shown in Fig. 19, the distribution curves of hydrogen volume fraction along the axial direction of the leakage orifice at the monitoring point after 100 s of leakage exhibit clear regularity under different pipeline pressures. Analysis of the curves indicates that as the pipeline pressure increases, the peak value of hydrogen volume fraction gradually rises: 71.0% at 0.3 MPa, 75.1% at 0.5 MPa, 79.8% at 0.8 MPa, and 83.9% at 1.0 MPa. In addition, the curves show that the higher the pipeline pressure, the wider the region of high hydrogen concentration and the larger the diffusion-affected area. For example, under the condition of 1.2 MPa, the hydrogen volume fraction maintains a high level over a wider distance range, whereas at 0.3 MPa, high concentration only occurs near the leakage orifice and drops rapidly as the distance increases, indicating a smaller diffusion-affected area. This is because the increase in pipeline pressure directly raises the hydrogen flow velocity and leakage rate at the orifice, resulting in more hydrogen escaping into the soil per unit time, which significantly increases the peak volume fraction at the monitoring point. At the same time, higher pressure provides a stronger driving force for hydrogen diffusion, pushing hydrogen to diffuse further in the soil and expanding the range of high-concentration regions. In summary, pipeline pressure not only determines the peak concentration of leaked hydrogen, but also significantly affects its diffusion capacity and affected range in the soil. Under high-pressure conditions, the safety risk associated with hydrogen leakage is greater.

Leakage orifice shape

As shown in Fig. 20, under the condition of equal leakage orifice area, three different shapes—circular, radial rectangular slit, and axial rectangular slit—were used to simulate the radial distribution of hydrogen volume fraction after 100 s of leakage from a buried pure hydrogen pipeline. The contour plots indicate that the shape of the leakage orifice has a significant impact on both the diffusion pattern and the spatial distribution of the leaked gas. In terms of diffusion-affected range, the axial rectangular slit exhibits the largest diffusion range, followed by the radial rectangular slit, while the circular orifice has the smallest affected area. Specifically, for the axial rectangular slit, the leaked gas is highly concentrated along the vertical direction of the orifice, forming a distinct peak-shaped region, and high-concentration hydrogen has already reached the ground surface, demonstrating strong penetrability. The radial rectangular slit also shows a certain peak-shaped distribution, but the peak value is less pronounced than that of the axial slit. Although the leaked gas approaches the ground surface, it is mainly at low concentrations. In contrast, the circular orifice produces a more diffuse, cloud-like distribution, with hydrogen not yet reaching the ground surface.

This is because different orifice shapes alter the directionality and diffusion pathways of the escaping gas. The axial rectangular slit, due to its elongated structure, provides a more direct vertical channel for the gas, allowing hydrogen to rise rapidly in the vertical direction, resulting in high-concentration gas reaching the

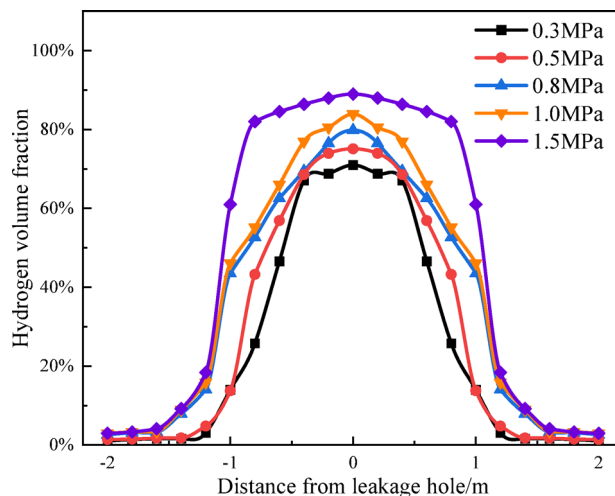


Fig. 19. Axial distribution curves of hydrogen volume fraction at the monitoring point after 100 s of leakage under different pipeline pressures.

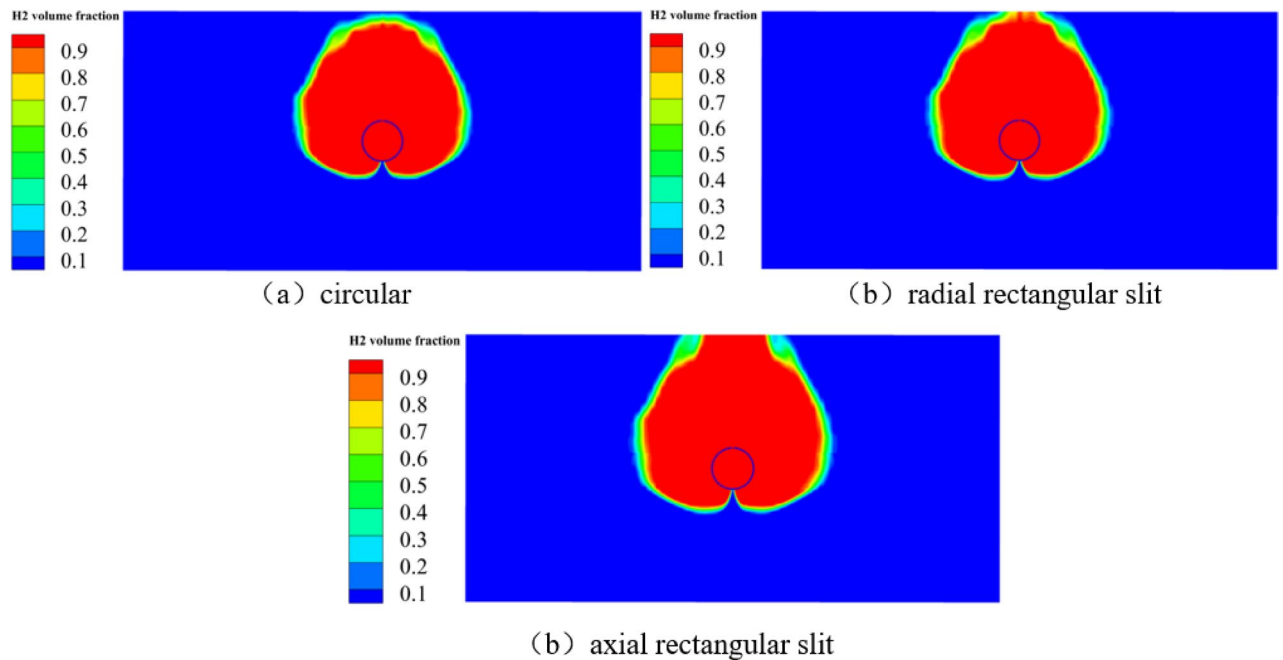


Fig. 20. Radial hydrogen volume fraction distribution contours at 100 s after leakage for different leakage orifice shapes.

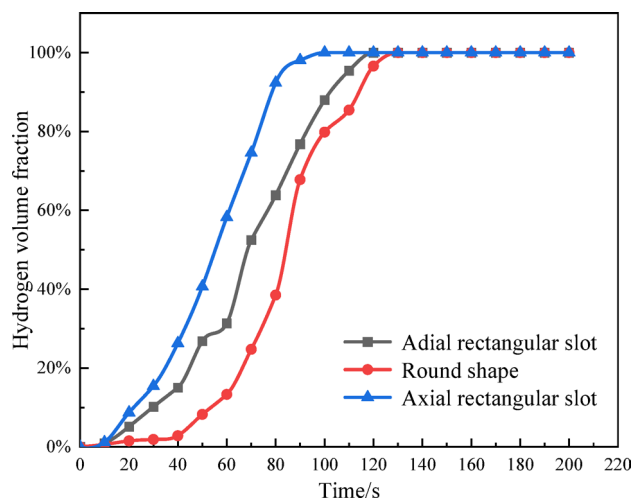


Fig. 21. Variation of hydrogen volume fraction with time at the monitoring point under different leakage orifice shapes.

surface more quickly and expanding the diffusion range. The radial rectangular slit mainly promotes radial diffusion, leading to a more dispersed gas distribution and lower concentration peaks. The circular orifice, on the other hand, allows for isotropic diffusion, with hydrogen spreading relatively evenly in all directions within the soil, resulting in a slower diffusion rate and a smaller affected range, as well as a reduced ability to reach the surface compared to the rectangular slits. These results demonstrate that the shape of the leakage orifice has a significant influence on the diffusion behavior of hydrogen leakage. In particular, the high-risk axial slit form requires special attention due to its pronounced safety hazards.

As shown in Fig. 21, at a monitoring point located 0.35 m vertically above the leakage orifice, the time-history curves of hydrogen volume fraction during the leakage process of a buried pure hydrogen pipeline were recorded for different leakage orifice shapes. The results show that within 200 s, the time required for the hydrogen volume fraction at the monitoring point to reach saturation varies with the orifice shape: the axial rectangular slit reaches saturation the fastest (about 100 s), followed by the radial rectangular slit (about 120 s), and the circular orifice is the slowest (about 130 s). This order is consistent with the observed trends in diffusion range and rate in the contour plots. In addition, the trends in hydrogen volume fraction for the three orifice types are generally similar,

but for the circular orifice, there is almost no significant change in hydrogen volume fraction at the monitoring point within the first 0–40 s. This suggests that in the early stage of leakage, hydrogen may accumulate locally near the orifice, resulting in high concentrations mainly around the leakage orifice and not rapidly diffusing to the monitoring point.

As shown in Fig. 22, after 100 s of leakage, the distribution curves of hydrogen volume fraction along the axial direction of the leakage orifice at the monitoring point reveal the significant impact of different leakage orifice shapes on hydrogen diffusion behavior. Analysis of the distribution curves shows that for the radial rectangular slit, circular orifice, and axial rectangular slit, the hydrogen volume fraction first increases and then decreases. Among them, the axial rectangular slit exhibits the highest peak value, reaching 100%; the peak value for the radial rectangular slit is 88.0%; and for the circular orifice, it is 79.8%. Beyond the 0 m position from the monitoring point, the hydrogen volume fraction for the axial rectangular slit decreases more slowly, with a relatively gentle curve, indicating that the hydrogen near the monitoring point is nearly saturated and maintains a high concentration distribution. In contrast, the volume fractions for the radial rectangular slit and circular orifice decrease much more rapidly after 1 m, especially for the circular orifice, where the hydrogen volume fraction quickly drops to a low level. Further observation shows that the axial rectangular slit has the widest hydrogen distribution range, with the volume fraction still remaining high even at 1.5 m from the leakage orifice; whereas for the radial rectangular slit and circular orifice, the distribution range is smaller, and the volume fraction has already dropped to a low value at 1 m.

This is mainly due to the influence of the geometric shape of the leakage orifice on the gas diffusion pathway and diffusion efficiency. The larger the aspect ratio of the orifice, the wider the distribution range of the gas near the orifice and the weaker the accumulation effect, which is beneficial for the sustained diffusion of hydrogen, resulting in faster diffusion speed and a larger affected area. The axial rectangular slit, being parallel to the pipeline axis, has a larger contact area with the soil, providing a smoother escape path for hydrogen and reducing accumulation and suppression effects near the orifice. Therefore, it exhibits a higher peak value and a wider distribution range. In comparison, the radial rectangular slit, due to the influence of pipeline curvature, has a slightly smaller contact area with the soil, and the accumulation and suppression effects near the orifice are relatively stronger, resulting in slightly lower diffusion speed and range than the axial slit. The circular orifice allows for isotropic diffusion, but the diffusion path faces greater resistance, making gas more likely to accumulate near the orifice and suppress subsequent diffusion, leading to a lower peak value and a smaller distribution range. In summary, the geometric shape of the leakage orifice significantly affects the diffusion characteristics of hydrogen leaking from buried pipelines in soil. Axial rectangular slits with a large aspect ratio facilitate rapid and wide-range diffusion of hydrogen, while radial slits and circular orifices exhibit relatively weaker diffusion capabilities.

Different hydrogen blending ratios

As shown in Fig. 23, the hydrogen blending ratios in the pipeline fluid were set to 100%, 80%, 60%, 40%, 20%, and 0%, respectively, and the model was used to simulate the radial distribution of gas volume fraction after 120 s of leakage under different hydrogen blending ratios. Observation of the contour plots reveals that the overall geometric shape of the gas distribution under different blending ratios is quite similar, all exhibiting a symmetrical and nearly circular diffusion pattern. When the hydrogen blending ratio is 0% (i.e., the leaked gas is pure methane), the diffusion in the horizontal direction is more pronounced, resulting in an elliptical distribution in the contour plot. As the hydrogen blending ratio increases, the diffusion range of the gas gradually expands, with the contour plots covering a larger area under higher hydrogen blending ratios. This is due to the physical property differences between hydrogen and methane: hydrogen has a much higher diffusion coefficient and lower density than methane, allowing it to diffuse more quickly and farther into the surrounding soil under

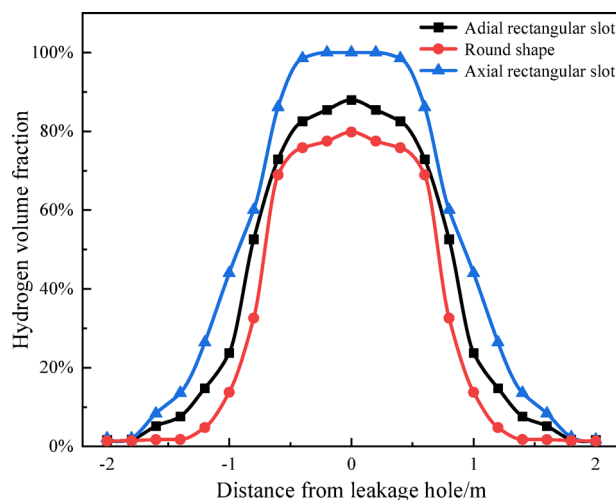


Fig. 22. Axial distribution curves of hydrogen volume fraction at the monitoring point after 100 s of leakage for different leakage orifice shapes.

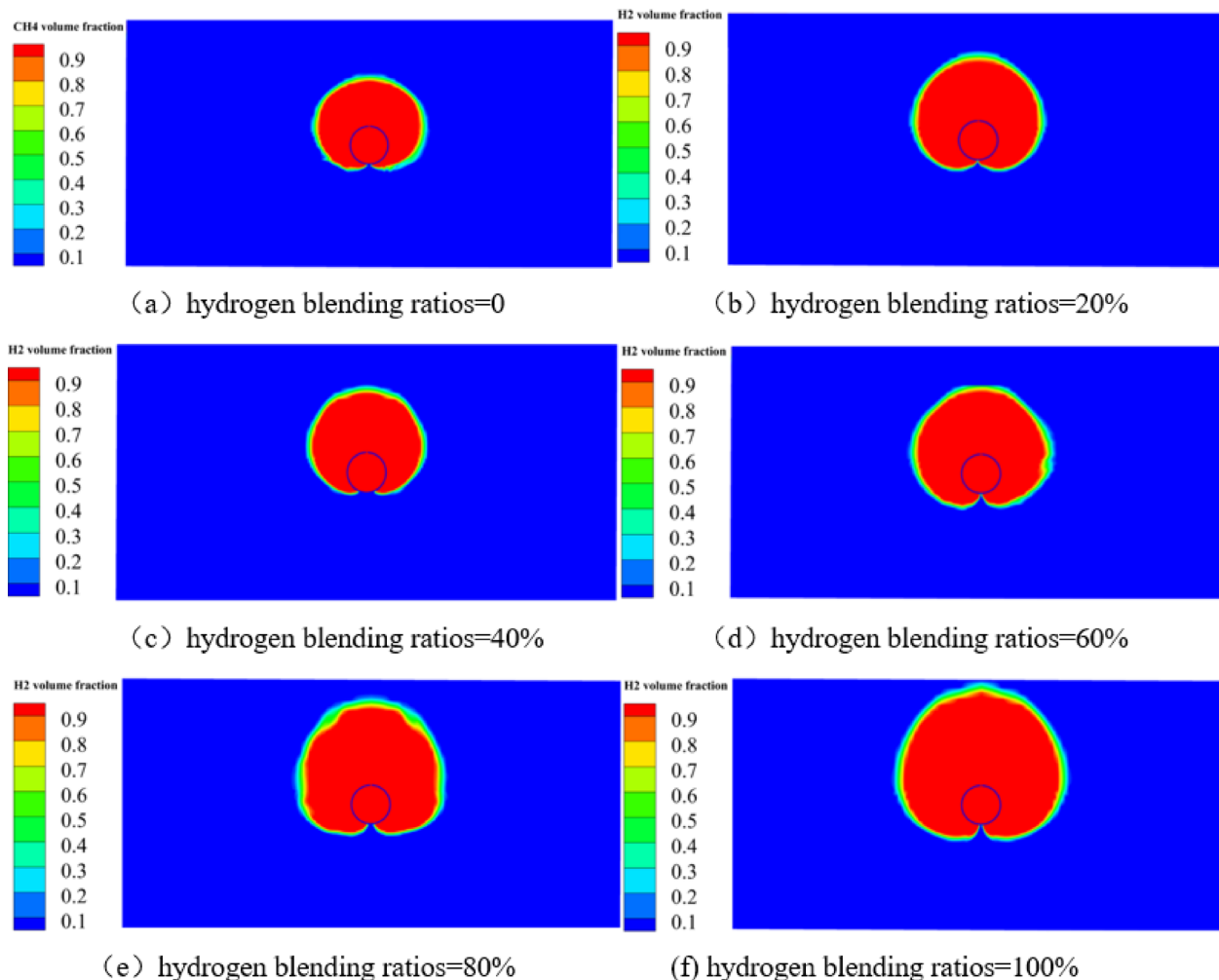


Fig. 23. Radial distribution contours of hydrogen volume fraction after 120 s of leakage for different hydrogen blending ratios.

the same conditions. When the hydrogen blending ratio increases, the hydrogen content in the leaked gas rises, enhancing the overall diffusion ability and thus significantly expanding the diffusion range. In contrast, when the blending ratio is 0%, methane's diffusion capacity is weaker and it tends to migrate more horizontally, leading to an elliptically stretched distribution in the contour plot. Therefore, changes in gas composition directly affect the diffusion behavior of the leaked gas in soil: the higher the hydrogen blending ratio, the faster the diffusion speed and the larger the affected area of the leakage.

As shown in Fig. 24, the dynamic curves of gas concentration at a soil monitoring point directly above the leakage orifice within 200 s after pipeline leakage are presented for six different hydrogen blending ratios (0%, 20%, 40%, 60%, 80%, and 100%). The curves indicate that the hydrogen blending ratio significantly affects the time required for the gas at the monitoring point to reach saturation. Specifically, for blending ratios of 0%, 20%, 40%, 60%, 80%, and 100%, the monitoring point reaches saturation at approximately 200 s, 180 s, 170 s, 150 s, 140 s, and 130 s, respectively. In the initial 0–40 s, the increase in gas concentration is relatively slow. After 40 s, the diffusion rate accelerates significantly, and the concentration eventually stabilizes at different time points, indicating that the gas volume fraction at the monitoring point has essentially reached saturation. Overall, as the hydrogen blending ratio increases, the growth rate of gas volume fraction becomes faster. Among them, the 100% hydrogen blending ratio (i.e., pure hydrogen) shows the fastest rise and reaches saturation earliest. This demonstrates that under high hydrogen blending ratios, the diffusion capacity of the leaked gas in the soil is stronger, enabling it to reach and saturate the soil pores around the monitoring point more quickly.

As shown in Fig. 25, the axial distribution curves of hydrogen-blended natural gas volume fraction at the monitoring point after 120 s of leakage under different hydrogen blending ratios generally exhibit a Gaussian distribution pattern. Specifically, with increasing hydrogen blending ratio, the peak value of the hydrogen-blended natural gas volume fraction gradually increases: for pure hydrogen (100% blending ratio), the peak is 96.6%; for blending ratios of 80%, 60%, 40%, and 20%, the peaks are 91.7%, 88.7%, 78.7%, and 75.6%, respectively; while for 0% blending ratio (pure methane), the peak is 75.6%. The shapes of the distribution curves are basically similar under different blending ratios, but at higher hydrogen blending ratios, the peak is higher and the distribution

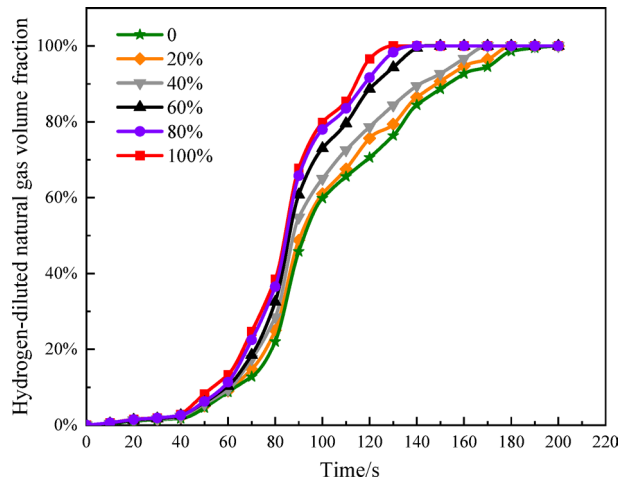


Fig. 24. Variation of hydrogen-blended natural gas volume fraction with time at the monitoring point within 200 s after pipeline leakage for different hydrogen blending ratios.

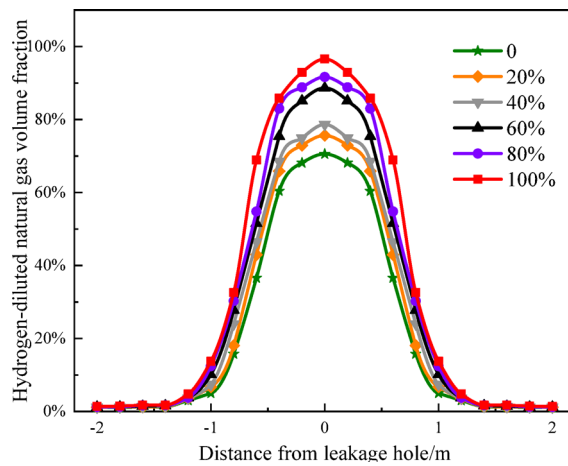


Fig. 25. Axial distribution curves of hydrogen-blended natural gas volume fraction at the monitoring point after 120 s of leakage under different hydrogen blending ratios.

Scenario (Case)	D (mm)	Porosity	t_{LEL} (s)	Diffusion Rate Change	Safety Implication
Reference (1)	5	0.43	≈ 115	Baseline	Standard soil conditions.
High Porosity (12)	5	0.55	≈ 75	34.8% faster	Soil type E presents the highest safety risk.
Low Porosity (11)	5	0.3	≈ 200	73.9% slower	Denser soil significantly delays risk onset.
Large Orifice (4)	10	0.43	≈ 60	47.8% faster	Orifice size is a dominant risk factor.

Table 3. The time required for hydrogen volume fraction to reach LEL under different working conditions.

range is slightly wider. This phenomenon is mainly attributed to the differences in physical properties between hydrogen and methane. Hydrogen has a higher diffusion coefficient and lower molecular mass, which allows it to diffuse and migrate more rapidly in the soil medium. As the hydrogen blending ratio increases, the overall diffusion capacity of the mixed gas is enhanced, enabling the leaked gas to reach the monitoring point more quickly and resulting in a faster saturation of the gas volume fraction at the monitoring point. Therefore, the higher the hydrogen blending ratio, the greater the peak volume fraction at the monitoring point, the faster the gas diffuses, and the wider the affected area. In summary, the high diffusivity of hydrogen is the fundamental reason for the increased peak volume fraction and improved diffusion efficiency under high hydrogen blending ratios.

Discussion

This section moves beyond the descriptive presentation of simulation outcomes to provide an in-depth quantitative analysis and mechanistic interpretation of the observed phenomena, as well as to discuss the practical safety implications of the results.

Quantitative analysis of surface hazard time (Time to LEL)

A primary goal of leakage modeling for buried pipelines is to predict the time required for the gas concentration to reach hazardous levels at the ground surface, representing the onset of explosion risk. For hydrogen, the Lower Explosive Limit (LEL) is defined as 4% volume fraction. We analyzed the time required (t_{LEL}) for the hydrogen volume fraction to reach the LEL at the monitoring point located on the ground surface ($y=2$ m directly above the orifice).

This quantitative analysis confirms that the time available for leak detection and emergency response is drastically reduced by factors that decrease soil resistance (high porosity/particle size) or increase mass flow rate (large orifice/high pressure).

Mechanistic interpretation of key influencing factors

Effect of Leakage Orientation (Buoyancy): The significant difference observed between upward and downward leakage (Sect. 3.2) is primarily governed by the extreme buoyancy of hydrogen ($M_{H_2}=2$ g/mol) relative to air ($M_{Air}=29$ g/mol). The upward leakage is strongly assisted by the buoyancy-driven flow, which superimposes onto the pressure-driven Darcy flow. In the downward scenario, the initial momentum is opposed by buoyancy, leading to a temporary high-concentration zone below the pipe that quickly dissipates as the gas reverses direction to migrate upwards. This confirms that buoyancy is the dominant long-term driving force governing hydrogen migration in soil.

Effect of Orifice Shape (Flow Channeling): The ranked diffusion performance (axial slit > radial slit > circular hole) is mechanistically explained by the effective flow path area and the resulting channeling effect.

Axial Slit (Case 23): Due to its elongation parallel to the pipeline axis, it maximizes the contact area with the soil directly above the pipe (in the y -direction), effectively creating a larger, more direct, two-dimensional vertical escape channel. This minimal resistance path accelerates the vertical diffusion, leading to the highest concentration peak and the fastest LEL.

Circular Hole (Case 1): Provides isotropic leakage but the narrowest immediate vertical path, leading to local pressure accumulation and higher resistance.

Effect of Soil Properties (Scaling Law): The strong dependence of t_{LEL} on soil porosity and particle size (Sect. 3.4) is directly related to the hydraulic conductivity of the porous medium. In the low-pressure range, hydrogen diffusion is largely constrained by the viscous resistance coefficient (α). The relationship between gas diffusion rate (R) and soil porosity (ϕ) and permeability (K) can be approximated by a simplified scaling law:

$$R \propto \frac{\phi K}{\mu} \cdot \frac{\Delta P}{L_{burial}} \quad (1)$$

Where permeability K is highly dependent on particle size, and porosity ϕ directly reflects the available volume fraction for flow. The simulation results quantitatively validate this physical mechanism: higher porosity (ϕ) and larger particle size (leading to smaller α and β) result in significantly reduced resistance coefficients (Table 2, comparing A, D, E), leading to a direct and non-linear acceleration of hydrogen migration towards the surface.

Model assumptions and limitations

The following limitations should be considered when applying these results to field conditions:

1. **Isothermal Assumption:** The model assumes an isothermal process. In reality, large leaks cause significant Joule-Thomson cooling, which could influence gas density and viscosity, slightly slowing diffusion in the immediate vicinity of the leak.
2. **Soil Homogeneity:** The soil is treated as homogeneous, dry, and isotropic. Field soil is heterogeneous and its properties (especially moisture content) vary, which would introduce greater resistance and channeling effects than modeled here.
3. **Pipe Degradation:** The simulation assumes a fixed orifice size, neglecting the possibility of crack propagation or wear over time, which would further accelerate the leakage rate.

Conclusions

This study employed a systematic numerical simulation method to investigate the diffusion characteristics of small-hole leakage from buried pure hydrogen and hydrogen-blended natural gas pipelines. The model was successfully validated against the established VDW-EOS theoretical model for mass flow rate calculation (with a 5.2% deviation). The key findings and practical implications are summarized as follows:

1. **Dominance of Flow Rate and Orifice Geometry:** An increase in leakage orifice diameter (e.g., from 5 mm to 10 mm) significantly accelerates the onset of hazard, reducing the time to reach maximum concentration at the monitoring point from 130 s to 80 s. Among the shapes tested, the axial rectangular slit presents the highest risk due to effective vertical channeling, demonstrating superior diffusion performance (axial slit > radial slit > circular hole).

2. Criticality of Soil Properties (Safety Benchmark): Soil characteristics are the most crucial factor controlling the diffusion risk. An increase in soil porosity (from 0.43 to 0.55) significantly accelerates the diffusion rate, reducing the Time to LEL (4%) at the ground surface from 115 s to approximately 75 s. This difference must be accounted for in establishing pipeline inspection intervals and surface monitoring strategies.
3. Buoyancy Effect: Upward-oriented leakage is confirmed as the highest risk scenario, as the buoyancy force of hydrogen assists the vertical migration. This effect is far more influential than small variations in pipeline burial depth.
4. Hydrogen Blending Ratio: As the hydrogen blending ratio increases (from 0% to 100%), the gas peak volume fraction at the monitoring point rises (from 75.6% to 96.6%), and the time required to reach concentration saturation shortens (from 200 s to 130 s). This validates that the high diffusivity of hydrogen fundamentally enhances the overall safety risk of the gas mixture.
5. Engineering Application: The established quantitative relationships between t_{LEL} and soil parameters provide a crucial safety benchmark for emergency planning and the design of localized surface monitoring systems for low-pressure hydrogen distribution networks. Future work should incorporate transient thermal effects and soil moisture content for full-scale risk assessment.

Data availability

The datasets supporting the findings and conclusions of this article, including all raw numerical simulation output files and processed data used to generate the figures (Figs. 4, 5, 6, 7, 8, 9, 10, 11, 12, 13, 14, 15, 16, 17, 18, 19, 20, 21, 22, 23, 24 and 25) and tables (Tables 1, 2 and 3), are available from the corresponding author, Dr. Longfei Dong (Email: [2018010@sdipt.edu.cn]), upon reasonable request. Furthermore, all key quantitative data are included within this published article and its supplementary information files.

Received: 11 August 2025; Accepted: 4 November 2025

Published online: 12 December 2025

References

1. Li, D. *Consequence Assessment of Hydrogen-Blended Natural Gas Leakage and Explosion in Typical Confined Spaces [D]* (Chongqing University, 2021).
2. Meng, S. *Research on Pipeline Leakage Monitoring and Early Warning in Unattended Natural Gas Stations [D]* (Guizhou University, 2023).
3. Hu, W. P. et al. Numerical simulation of leakage and diffusion from buried pure hydrogen/hydrogen-blended natural gas pipelines[J]. *Oil & Gas Storage and Transportation*, 42(10): 1118–1127. (2023).
4. Zhang, W. & Zhao, G. Leakage and diffusion characteristics of underground hydrogen pipeline. *Petroleum* **10**, 319–325 (2024).
5. Wang, J. et al. Numerical simulation analysis of buried pipeline leakage. *Sci. Technol. Eng.* **20**, 13660–13666 (2020).
6. Li, F. et al. Key technologies and progress in the safe long-distance transportation of hydrogen-blended natural gas pipelines. *Mech. Eng.* **45** (02), 230–244 (2023).
7. Yan, M., Li, J. & Guan, Y. Rupture leakage model for a natural gas pipeline[J]. *J. Pipeline Syst. Eng. Pract.* **14** (1), 04022060 (2023).
8. Feng, Y. et al. Risk assessment and simulation of gas pipeline leakage based on Markov chain theory[J]. *J. Loss Prev. Process Ind.* **91**, 105370 (2024).
9. Zhang, B. et al. Study of multisource leakage diffusion and explosion risk of underground natural gas pipelines[J]. *J. Pipeline Syst. Eng. Pract.* **15** (1), 04023056 (2024).
10. Zhu, J. et al. Leakage and diffusion behavior of a buried pipeline of hydrogen-blended natural gas[J]. *Int. J. Hydrog. Energy.* **48** (30), 11592–11610 (2023).
11. Liu, C. et al. *Quantitative Assessment of Leakage Orifices Within Gas Pipelines Using a Bayesian network[J]* Vol. 209, 107438 (Reliability Engineering & System Safety, 2021).
12. Ndalila, P. D. et al. Modeling dynamic pressure of gas pipeline with single and double leakage[J]. *IEEE Sens. J.* **21** (9), 10804–10810 (2021).
13. Li, F. et al. Noise-Pressure interaction model for gas pipeline leakage detection and location[J]. *Measurement* **184**, 109906 (2021).
14. Yan, M. et al. A buried gas pipeline leakage Model[J]. *J. Pipeline Syst. Eng. Pract.* **15** (4), 04024046 (2024).
15. Chang, W. et al. Numerical study of the soil temperature field affected by natural gas pipeline Leakage[J]. *Processes* **13** (1), 36 (2024).
16. Duan, P. F. et al. *Leakage and Diffusion Characteristics of hydrogen-blended Natural Gas in Utility corridors[J]* Vol. 42, 901–909 (Oil & Gas Storage and Transportation, 2023), 08.
17. Wu, X. et al. Mathematical model of leakage during pressure tests of oil and gas pipelines[J]. *J. Pipeline Syst. Eng. Pract.* **6** (4), 04015001 (2015).
18. Wang, L. et al. Numerical study of leakage characteristics of hydrogen-blended natural gas in buried pipelines[J]. *Int. J. Hydrog. Energy.* **49**, 1166–1179 (2024).
19. Nourollahi, E., Rahimi, A. B. & Davarpanah, E. Simulation of Gas Pipelines Leakage Using Modified Characteristics Method[J]. (2012).
20. Xu, Q., Zhang, L. & Liang, W. Acoustic detection technology for gas pipeline leakage[J]. *Process Saf. Environ. Prot.* **91** (4), 253–261 (2013).
21. Li, T. *Study on Flame Instability and Explosion Characteristics of Hydrogen Pipeline Leakage Combustion [D]* (Jiangsu University of Science and Technology, 2022).
22. Zhao, A. et al. Basic acoustic wave Time-Frequency parameters of buried gas pipeline Leakage[J]. *J. Pipeline Syst. Eng. Pract.* **15** (4), 04024045 (2024).
23. Yang, J. & Zhang, Y. Q. Forward simulation study of leakage in buried oil pipelines[J]. *Electron. Meas. Technol.* **44** (15), 136–141 (2021).
24. Hao, Y. et al. Leakage signal analysis of urban gas pipeline based on improved variational mode decomposition[J]. *Int. J. Pattern recognit. Artif. Intell.* **34** (13), 2058018 (2020).
25. Wang, D. et al. Research on gas pipeline leakage model identification driven by digital twin[J]. *Syst. Sci. Control Eng.* **11** (1), 2180687 (2023).
26. Liang, W. et al. Gas pipeline leakage detection based on acoustic technology[J]. *Eng. Fail. Anal.* **31**, 1–7 (2013).
27. Gong, X. et al. A leak sample dataset construction method for gas pipeline leakage estimation using pipeline studio[C]//2021 International Conference on Advanced Mechatronic Systems (ICAMechS). IEEE, : 28–32. (2021).
28. Yu, S. et al. Acoustic microfiber sensor for gas pipeline leakage detection[J]. *Measurement* **218**, 113242 (2023).

29. Han, K. S. & Yu, J. J. Simulation experiment for gas pipeline leakage Detection[J]. *Adv. Mater. Res.* **805**, 1502–1506 (2013).
30. Yue, B. et al. Classification of hydrate blockage and pipeline leakage in natural gas pipelines based on EMD and SVM[J]. *J. Pipeline Syst. Eng. Pract.* **13** (1), 05021012 (2022).
31. Liu, Z. et al. Experimental study on the leakage temperature field of buried CO₂ pipelines[J]. *Environ. Sci. Pollut. Res.* **30** (27), 70288–70302 (2023).

Author contributions

Longfei Dong and Xin Pang wrote the main manuscript text and Rui Zhang prepared Figs. 1, 2, 3, 4, 5, 6, 7, 8, 9 and 10. All authors reviewed the manuscript.

Funding

This work was supported by Natural Science Foundation of Dongying, China (Grant No. 2023ZR04), the Science Development Funding Program of Dongying of China (Grant No. DJ2023004) and Dongying City Science and Technology Innovation Major Project (Science and Technology Development Guidance Scheme) (Grant No. 2024ZDJH75).

Declarations

Competing interests

The authors declare no competing interests.

Additional information

Correspondence and requests for materials should be addressed to L.D.

Reprints and permissions information is available at www.nature.com/reprints.

Publisher's note Springer Nature remains neutral with regard to jurisdictional claims in published maps and institutional affiliations.

Open Access This article is licensed under a Creative Commons Attribution-NonCommercial-NoDerivatives 4.0 International License, which permits any non-commercial use, sharing, distribution and reproduction in any medium or format, as long as you give appropriate credit to the original author(s) and the source, provide a link to the Creative Commons licence, and indicate if you modified the licensed material. You do not have permission under this licence to share adapted material derived from this article or parts of it. The images or other third party material in this article are included in the article's Creative Commons licence, unless indicated otherwise in a credit line to the material. If material is not included in the article's Creative Commons licence and your intended use is not permitted by statutory regulation or exceeds the permitted use, you will need to obtain permission directly from the copyright holder. To view a copy of this licence, visit <http://creativecommons.org/licenses/by-nc-nd/4.0/>.

© The Author(s) 2025